Spectrochimica Acta Part A: Molecular and Biomolecular Spectroscopy 295 (2023) 122571

Contents lists available at ScienceDirect

Spectrochimica Acta Part A:
Molecular and Biomolecular Spectroscopy

journal homepage: www.journals.elsevier.com/spectrochimica-acta-part-a-molecular-and-biomolecular-spectroscopy

Comparing the effect of electron beam, beta and ultraviolet C exposure on the luminescence emission of commercial dosimeters

C. Boronat [a,b,*], V. Correcher [b], J.C. Bravo-Yagüe [a], I. Sarasola-Martin [b], J. Garcia-Guinea [c], J.F. Benavente [b]

[a] UNED, Av. de Esparta s/n, 28232 Madrid, Spain
[b] CIEMAT, Av. Complutense 40, 28040 Madrid, Spain
[c] MNCN-CSIC, J. Gutierrez Abascal 2, 28006 Madrid, Spain

HIGHLIGHTS

- TLD-100, TLD-200, TLD-400 and GR-200 dosimeters could be potentially used in the field of UV Dosimetry.
- Luminescence characterization (CL and TL) of these dosimeters exposed to electro beam, beta and Ultraviolet C radiation were here discussed in detail.
- TL glow curves allows to discriminate groups of components of the TLDs exposed to beta and UVC radiation.
- CL emissions differ considerably in the shape and intensity due to their chemical compositions.
- The estimation of the kinetic parameters could be studied by means of the Computerised Glow Curve Deconvolution (CGCD) method.

GRAPHICAL ABSTRACT

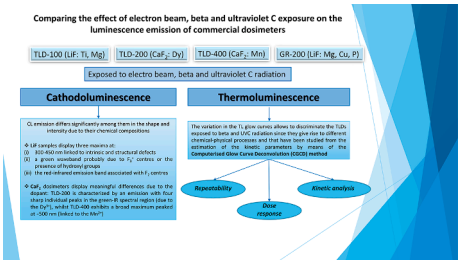

ARTICLE INFO

Keywords:
Luminescence
Ultraviolet
Dosimeters
Kinetics Analysis
LiF
CaF_2

ABSTRACT

This paper reports on the luminescence characterization of TLD-100 (LiF: Ti, Mg), TLD-200 (CaF_2: Dy), TLD-400 (CaF_2: Mn) and GR-200 (LiF: Mg, Cu, P) dosimeters exposed to electro beam, beta and ultraviolet C radiation -UVC-. All of them show high sensitivity to radiation regardless of whether it is ionizing or partially ionizing radiation based on their luminescence properties (cathodoluminescence -CL- or thermoluminescence -TL-). CL emission differs significantly among them in shape and intensity due to their chemical compositions. LiF samples display three maxima at: (i) 300–450 nm linked to intrinsic and structural defects, (ii) a green waveband probably due to F_3^+ centres or the presence of hydroxyl groups and (iii) the red-infrared emission band associated with F_2 centres. However, CL spectra from the CaF_2 dosimeters display meaningful differences due to the dopant. TLD-200 is characterized by an emission with four sharp individual peaks in the green-IR spectral region (due to the Dy^{3+}), whilst TLD-400 exhibits a broad maximum peaked at-500 nm (linked to the Mn^{2+}). On the other hand, the variation in the TL glow curves allows to discriminate the TLDs exposed to beta and UVC radiation since they give rise to different chemical-physical processes and that have been studied from the estimation of the kinetic parameters by means of the Computerised Glow Curve Deconvolution (CGCD) method.

* Corresponding author at: UNED, Av. de Esparta s/n, 28232 Madrid, Spain.
E-mail address: cboronat9@alumno.uned.es (C. Boronat).

https://doi.org/10.1016/j.saa.2023.122571
Received 14 January 2023; Received in revised form 20 February 2023; Accepted 27 February 2023
Available online 3 March 2023

1. Introduction

Significant efforts are being carried out for the development of new materials that can be used as phosphors in the fields of, (i) industry sectors [1,2] (i.e. light-emitting diodes), pharmaceutical and medical field [3] (i.e. radiation safety protection and radiotheraphy), food industry [4,5] (i.e. decontamination and sterilization) and environmental analysis [4,6] (i.e. climate change and global warming), etc. Most of them, insulators and semiconductors, can also be employed for dosimetric purposes based on their luminescence properties including both thermoluminescence (TL) and cathodoluminescence (CL).

The main advantages of TL dosimeters for these applications are (i) their small physical size, (ii) they can be produced in different types (as powder, ribbons, single crystals, chips and teflon-impregnated discs [7]), (iii) their wide sensitive range (i.e. 1–100 Gy for the TLD-200 (CaF_2: Dy) and the high sensitivity of the TLD-400 (CaF_2: Mn) dosimeter to doses as low as 50 μGy and its simple glow curve [8,9]) and (iv) the resistance to corrosion and damage. In this case, LiF and CaF_2 matrices are of special interest in the field of luminescence dosimetry as they are able to incorporate many impurities (i.e. Ti, Mg, Cu, P, Dy, Mn, etc.) giving rise to defects, cluster formation, inclusions and valence changes that can act as traps for electrons and holes. They are not only involved in the luminescence mechanism, but can also affect to basic dosimetric properties, such as, dose response, sensitivity, trap structure or fading.

Thus, the composition and structure of these chips and their intrinsic characteristics and typomorphic properties can be determined by luminescence techniques, such as cathodoluminescence (CL) and thermoluminescence (TL) [10]. Intrinsic and extrinsic defects are potentially responsible for different luminescence emissions. They are generally noticed in insulator materials during excitation with ions, electrons, temperature, ultraviolet (UV) or ionizing radiation. Both CL and TL techniques supply information about the trapped charge recombination sites related to metastable defects inside the lattice depending on whether the detrapping process is due to electron exposure or heating respectively. Therefore, CL is a technique whereby light is emmited from an energetic electron beam, providing data about transient defects after irradiation on the surface of the lattice and is used in the identification of the migration and diffusion of some luminescent centers from the emission bands [11]. Furthermore, TL is a technique based on the emission of light from a solid sample such as insulator or semiconductor when it is heated after being irradiated by some kind of radiation such as gamma rays, beam of electrons, X-rays, cosmic rays, etc [7]. TL supplies information about the trapped charge recombination sites related to metastable defects inside the lattice if the detrapping process is due to heat. All factors entailed in the luminescence phenomena (i.e. lifetime, efficiency, emission spectra, etc.) are directly determined by the crystalline phase, which is mainly influenced by pressure and temperature. Thus, small variations in the lattice structure due to the presence of impurities, substituted ions, inclusions or surface defects in ppm concentrations show changes in the intensity and wavelength position the emission spectra.

Aditionally, UV radiation, specifically UVC (in the range from 100 to 280 nm), produces three-stage process that are directly related to the luminescence mechanism: (i) phototransfer of charges from deeper to shallower traps upon illumination [12], (ii) UVC is partially ionizing, namely a partial liberation of electrons from atoms and molecules, causing bond breaking (i.e. photodissociation and photooxidation processes) [13] and (iii) bleaching effect on the TL signal [14]. The phototransferred luminescence (PTTL) emission of a material is related to its UV-TL glow curve which has been previously exposed to ionizing radiation [12]. Such radiation causes free charges that are presented in the corresponding trapping states. This effect occurs when the electrons are thermally released from shallower traps and recombine radiatively at luminescence centers during a subsequent heating, giving rise to the PTTL signal.

Thus, this paper reports on the luminescence characterization of TLD-100 (LiF: Ti, Mg), TLD-200 (CaF_2: Dy), TLD-400 (CaF_2: Mn) and GR-200 (LiF: Mg, Cu, P) dosimeters exposed to electro beam, beta and Ultraviolet C radiation by means of (i) CL properties; (ii) a repeteability study and (iii) the dose response. On the other hand, the variation in the TL glow curves allows to discriminate groups of components of the TLDs exposed to beta and UVC radiation since they give rise to different chemical-physical processes and that have been studied from the estimation of the kinetic parameters using the Computerised Glow Curve Deconvolution (CGCD) method.

2. Materials and methods

LiF: Ti,Mg (TLD-100), CaF_2: Dy (TLD-200), CaF_2: Mn (TLD-400) dosimeters supplied by Harshaw Chemical Company (Ohio, USA) with sizes of $0.32 \times 0.32 \times 0.09$ cm^3 each and LiF: Mg,Cu,P (GR-200) discs of 4.5 Ø 0.8 mm^3 dimensions provided by Beijing Shiying Radiation Detector Works (China) were here studied. The luminescence emission of such materials was characterized by means of CL and TL techniques. The CL spectra, which covers a spectral range of 250–850 nm, were measured using a Gatan MonoCL3 detector with a PA-3 photomultiplier tube attached to the ESEM model XLS30. Samples were placed on polished slabs, at low-vacuum mode without coating to keep open way out to the CL emission that was collected and amplified using a retractable parabolic diamond mirror, with a distance of 15 mm between the sample and the bottom of the mirror. The excitation for CL measurements was provided at 27 kV electron beam. TL measurements were performed employing an automated RisØ TL reader model TL DA-12 provided with an EMI 9635 QA photomultiplier [15]. The emission was observed through a blue filter (a FIB002 of the Melles-Griot Company) where the wavelength is peaked at 320–480 nm; FWHM is 80 ± 16 nm; and peak transmittance is 60%. The TL reader is also supplied with a $^{90}Sr/^{90}Y$ source with a dose rate of 0.010 Gy/s calibrated against a ^{137}Cs photon source in a secondary standard laboratory. All the TL measurements were obtained using a linear heating rate of 5 °C/s from RT up to 400 °C in N_2 atmosphere. The UVC radiation effect was characterized by means of the TL properties of the abovementioned TLD detectors. Such dosimeters were exposed to a TUV-6 W Hg lamp (254.7 nm with an UV irradiance value at 10 cm of 0.03 W/m^2). The irradiator, developed at CIEMAT [16], allows to pre-select the irradiation time at a controlled temperature. The time between the end of UV irradiation and the TL measurement (10 min) is controlled to keep the fading constant.

2.1. CGCD analysis

Computerised Glow Curve Deconvolution (CGCD) was used to obtain kinetic parameters (Peak Maximum Temperature in °C -T_M-, Intensity of the maximum in a.u. -I_M-, Activation Energy in eV -E-, Frequency factor in s^{-1} -S- and Distribution wide in eV -σ-) from the experimental TL glow curves [17], employing a linear combinations of functions that can be expressed as follows:

$$I(T_j) = \sum_{n=1}^{N_{peaks}} f_{(n)}(T_j; I_M^{(n)}, T_M^{(n)}, E^{(n)}, \sigma^{(n)}) \quad (1)$$

i. Taking into account a First Order Kinetics (FOK) approach, $f_{(n)}$ (T_j; $T_M^{(n)}$, E, σ) function can be expressed as follows (Eq. (2) assuming a localized trap distribution with σ = 0.0 eV):

$$f(T_j; I_M, T_M, E) = I_M \cdot \exp\left(\frac{E}{K_b \cdot T_M} - \frac{E}{K_b \cdot T_j}\right) \cdot \exp\left\{\frac{E}{K_b \cdot T_M^2} \cdot \int_{T_M}^{T} e^{\frac{E}{K_b \cdot T_M} - \frac{E}{K_b \cdot T'}} \cdot dT'\right\} \quad (2)$$

ii Eq. (3) assuming a continuous trap distribution with σ > 0.0 eV:

$$f\left(T_j;I_M,T_M,E,\sigma\right)=I_M\frac{\int_{E_1}^{E_2}g(E)\cdot e^{\frac{-E}{K_b\cdot T}}\cdot\ exp\left\{\frac{E_0}{K_b\cdot T_M}\cdot e^{\frac{-E_0}{K_b\cdot T_M}}\int_{T_0}^{T}e^{-\frac{E}{K_b\cdot T'}}\bullet dT'\right\}dE}{\int_{E_1}^{E_2}g(E)\cdot e^{\frac{-E}{K_b\cdot T_M}}\cdot\ exp\left\{\frac{E_0}{K_b\cdot T_M}\cdot e^{\frac{-E_0}{K_b\cdot T_M}}\int_{T_0}^{T_M}e^{-\frac{E}{K_b\cdot T'}}\bullet dT'\right\}dE} \quad (3)$$

Where $g\ (E)$ is related to a trap contribution form considering a exponential distribution:

$$g(E)=\frac{1}{\sigma}\cdot e^{-\frac{E-E_0}{\sigma}} \quad (4)$$

Experimental glow curve fitting were developed using an iterative method based on the Levenberg –Marquardt algorithm to minimise the X^2 as described in Eq. (5):

$$X^2=\sum_{j=1}^{N_p}\left[I_j-\sum_{n=1}^{N_{peaks}}f_{(n)}\left(T_j;I_M^{(n)},T_M^{(n)},E^{(n)},\sigma^{(n)}\right)\right]^2=\sum_{j=1}^{N_p}\left[I_j-I(T_j)\right]^2 \quad (5)$$

Where I_j corresponds to the experimental values.

The frecuency factor S is obtained by Eq. (6):

$$S\left(s^{-1}\right)=\frac{\beta\cdot E}{K_b\cdot T^2{}_{MAX}}\cdot\ e^{\frac{E}{K_b\cdot T_{MAX}}} \quad (6)$$

Where $K_b=8.61\cdot10^{-5}$ eV/K is the Boltzmann constant and $\beta=5$ °C/s is the heating rate.

3. Results and discussion

3.1. Cathodoluminescence (CL) results

As illustrated in Fig. 1, CL spectral emission of TLD-100 **(a)**, TLD-200 **(b)**, TLD-400 **(c)** and GR-200 **(d)** dosimeters are measured at RT in the UV-IR range. TLD-100 (Fig. 1a) and GR-200 (Fig. 1d) display, at least, three groups of components consisting on: (i) a broad band in the range of 300–450 nm, which could be associated with the intrinsic emission of LiF, due to the recombination of an electron with a self-trapped hole or a V_k centre [18]; (ii) the green waveband could be linked to the F_3^+ emission band induced by the recombination of a released hole with an F_3 centre produced by the electron beam irradiation [19]; and (iii) the red-infrared emission band would be due to the F_2 centre in the LiF lattice [20]. There are several luminescence mechanisms that could consecutively give rise to (i) F absorption band excitation, (ii) recombination of a released hole with an F_2 centre, (iii) F_2 absorption band excitation or, (iv) the recombination of a released electron with an F_2^+ centre. The F centre (colour centre [21]) is formed when an electron is trapped in an anion vacancy, whilst the F_2 and F_3 centres are formed when two or three electrons are trapped in two or three anion vacancies beside to each other, respectively. Such colour centres have been observed not only in LiF, but also in alkaline-earth halides (CaF_2) crystals [22].

Otherwise, TLD-200 and TLD-400 exhibit CL glow curves that differs considerably in shape and intensity. The CL spectrum corresponding to TLD-200 (Fig. 1b) exhibits a broad waveband in the UV-blue region associated with structural defects linked to the CaF_2 lattice and, associated with the presence of the Dy^{3+} dopant, sharp peaks located in the UV-blue (450–500 nm), green-orange (550–600 nm), orange-red (650–690 nm) and infrared (740–775 nm) regions that could be respectively associated with $^4F_{9/2}\rightarrow{}^6H_{15/2}$, $^4F_{9/2}\rightarrow{}^6H_{13/2}$, $^4F_{9/2}\rightarrow{}^6H_{11/2}$ and $^4F_{9/2}\rightarrow{}^4F_{11/2}+{}^6H_{9/2}$ transitions. Several studies have shown that the emission peaks of this lanthanide ion are not dependent on the host material (i.e. $LaAlO_3$ [23], $Ca_3Y_2B_4O_{12}$ [24], La_2MoO_6 and $La_2Mo_2O_9$ [25], among others). Such emission involves two dominant bands: (i) the blue emission ($^4F_{9/2}\rightarrow{}^6H_{15/2}$) related to a magnetic dipole transition, which its intensity hardly deals with the crystal field and, (ii) the yellow-orange emission ($^4F_{9/2}\rightarrow{}^6H_{13/2}$) which has a hyper sensitive and electric dipole transition ($\Delta J=2$), that is strongly influenced by the crystal field

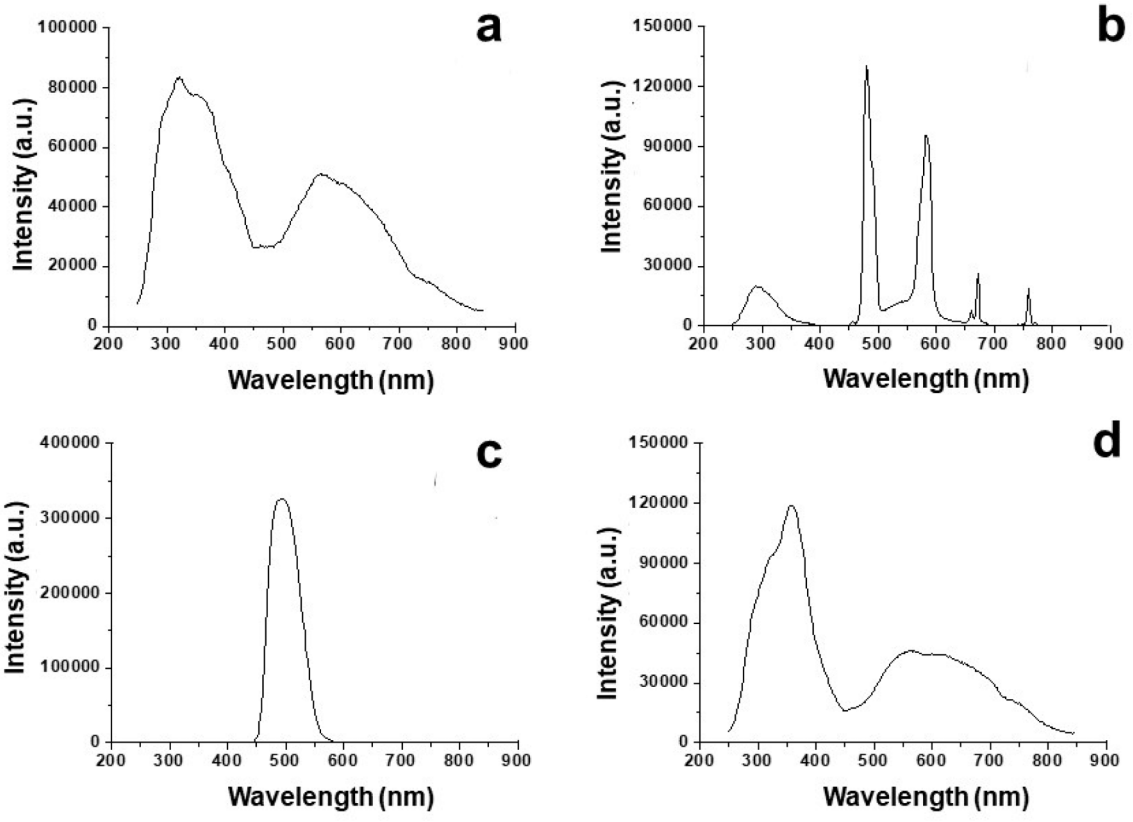

Fig. 1. Cathodoluminescence spectra of (a) TLD-100, (b) TLD-200, (c) TLD-400 and (d) GR-200 dosimeters measured at RT.

environment [26] and is only allowed without the presence of an inversion center. Thus, when the Dy^{3+} ion is located without an inversion center (low symmetry local site), the yellow-orange emission predominates in the luminescence spectrum. On the contrary, when the Dy^{3+} ion is located with an inversion center (high symmetry local site), the blue emission dominates over the yellow-orange one [23]. TLD-200 displays a higher blue emission ($^4F_{9/2} \rightarrow {}^6H_{15/2}$), with an intensity ratio of 3:2, indicating that the magnetic dipole transition dominates against the electric dipole transition.

Fig. 1c reveals that CL emission spectra of TLD-400 only displays a waveband centered at 490 nm so it is not possible to distinguish a broad waveband in the UV-blue region associated with the CaF_2 lattice. According to Topaksu et al., [9], it would be linked to Mn^{2+} impurities (1.7% in the TLD-400) that are placed in Ca^{2+} sites in the crystal lattice due to the transfer of electron-hole recombination energy close to $Mn^{2+} \leftrightarrows Mn^{3+}$ and subsequent relaxation from the excited state $[Mn^{2+} \leftrightarrows Mn^{3+}]^*$ to the ground state, which is caused by the transition $^4T_{1g}(^4G) \rightarrow {}^6A_{1g}(^6S)$ in the Mn^{2+} ($3d^5$) ions [27].

3.2. Thermoluminescence (TL) results

3.2.1. Repeatability

One of the required features of a potential dosimeter is its suitability for being reused without changes in the electron-hole trapping centres. In order to determine the stability of the TL signal, five successive cycles of irradiation (at 10 mGy for ionizing radiation and 40 min of UVC exposure) and readout (up to 400 °C) without applying a thermal annealing before each cycle were herein recorded (Figs. 2 and 3).

As ilustrated in Fig. 2, beta-induced TL gives rise to low dispersion between aliquots and cycles in all the materials, except in the GR-200 material, where the stability of the TL signal decreases linearly, up to 25% after 5 cycles. This behavior could be associated with a change of the matrix of the material after being irradiated and readout. It could be improved by supplying a thermal annealing between each measurement to recover the homogeneity and stability of the crystalline structure [28]. The rest of the dosimeters show a high stability of the glow emission with a dispersion never higher than 2.5% for TLD-100 and TLD-400 and lower than 1% for TLD-200. For that reason, the CaF_2: Dy (TLD-200) appears as the most acceptable dosimeter considering the TL stability under these conditions since there is not an eviction or an increase of electrons or holes from the ground state to non-radiative recombination centers.

As detailed in Fig. 3, the TL emission due to UVC exposure shows significant scattering between the batch of aliquots and the entire experiment (including all 5 cycles). TLD-100 and TLD-400 materials differ significantly in the stability of the TL signal (being 50% and 30% of dispersion between aliquots respectively) nevertheless, the dispersion reaches 70–80% among cycles for both samples. On the other hand, GR-200 exhibits an acceptable dispersion between aliquots (24%), though the evolution of the TL intensity increases linearly up to 60%; such effect could be partialy associated with the previously mentioned instability of the β reference signal. However, TLD-200 shows the lowest dispersion of all of them, 22% between aliquots and 50% among the cycles. Consequently, as previously explained in Fig. 2, CaF_2: Dy (TLD-200) would be suitable for measurements regarding thermal stability of the TL signal up to 400 °C at constant doses of 10 mGy. The uncertainties were calculated considering the classical GUM guidance assuming a confidence limit of 95% accuracy and standard deviation 1σ that is determined from the mean value of each group of 5 aliquots corresponding to each sample [29].

3.2.2. Dose response

The evolution of the TL emission when the exposure dose increases could determine if the electron hosted in the traps (initially empty) and

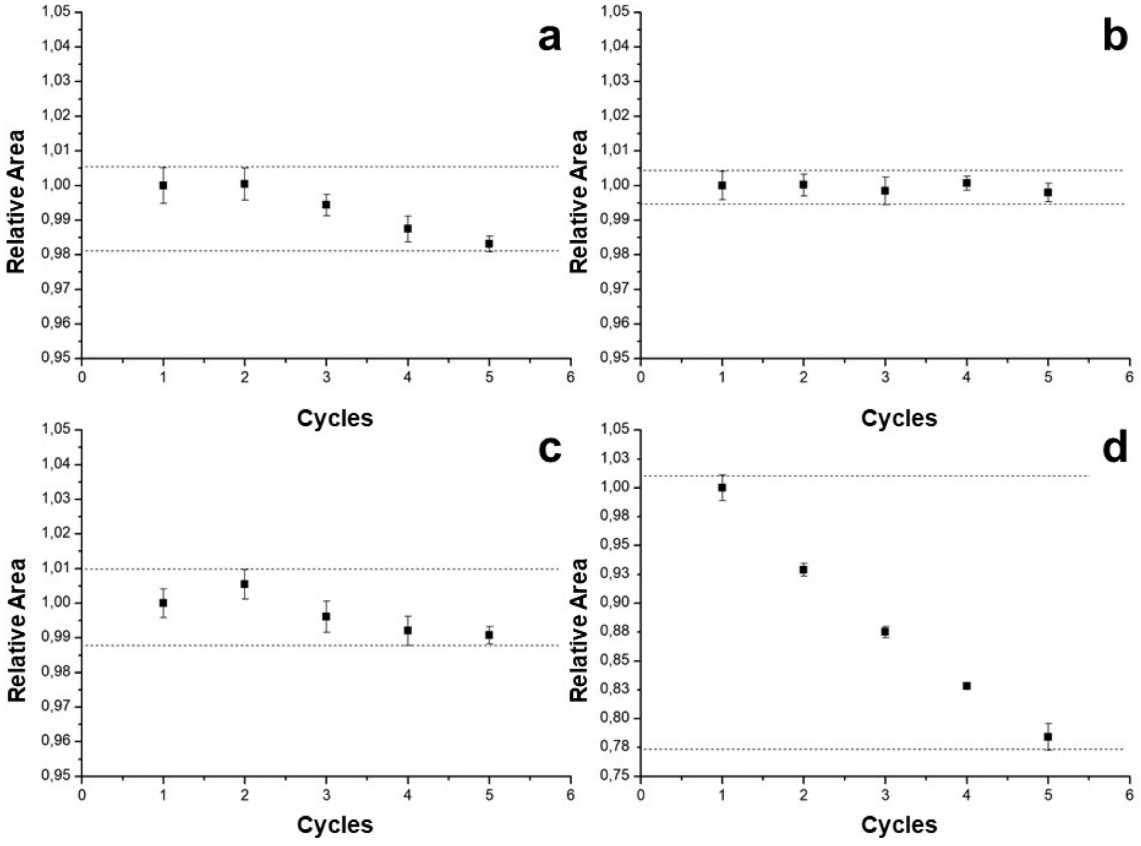

Fig. 2. Repeteability for 5 cycles using β radiation on (a) TLD-100, (b) TLD-200, (c) TLD-400 and (d) GR-200 dosimeters.

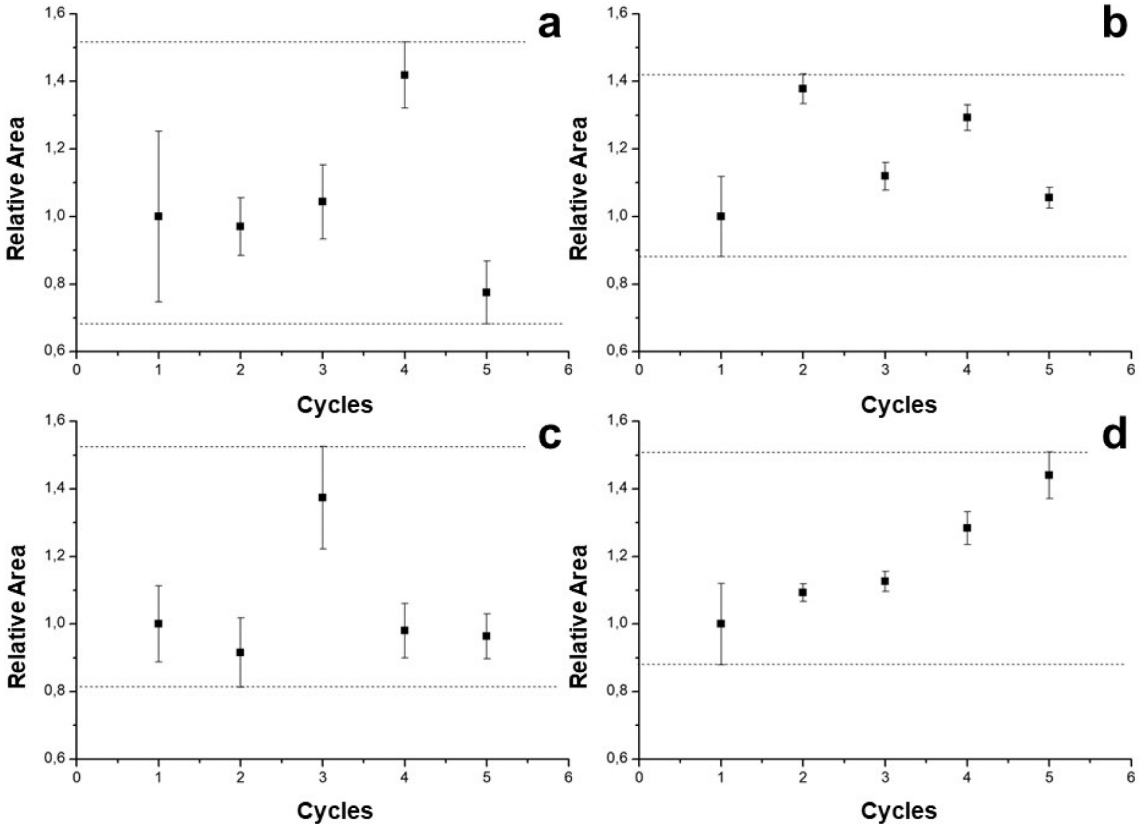

Fig. 3. Repeteability for 5 cycles using UVC radiation on (a) TLD-100, (b) TLD-200, (c) TLD-400 and (d) GR-200 dosimeters.

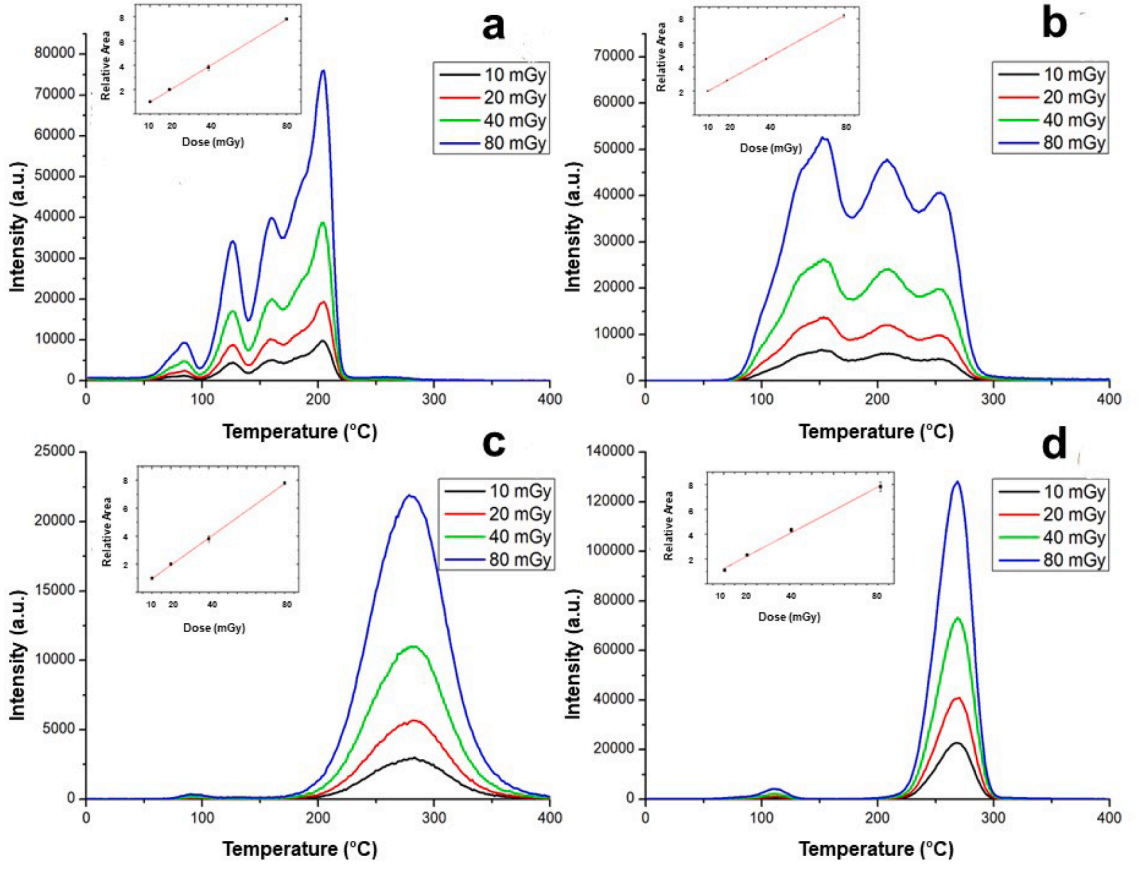

Fig. 4. Dose response of (a) TLD-100, (b) TLD-200, (c) TLD-400 and (d) GR-200 dosimeters exposed from 10 to 80 mGy of β irradiation.

the luminescence emission is proportional to the concentration of the filled traps with the absorbed dose. Additionally, if the position of the maxima does not shift, it is possible to assume first order kinetics for the TL process [30]. As observed in Fig. 4, the evolution of the TL emission of β-irradiated materials in the range of 10–80 mGy fits to an equation of the sort of: $= a_0 + b_0 \cdot x$, where y corresponds to the intensity of the TL signal, x is the given dose, a_0 is an independent coefficient and b_0 is the slope of the straight line with correlation coefficients over 0.996 (Table 1). None of the materials herein studied display a sublinearity or supralinearity in the range typically employed for personal dosimetry.

Otherwise, UVC-irradiated samples (Fig. 5), in the range of 10–120 min, display a sublinear evolution for TLD-100, TLD-200 and TLD-400 dosimeters that can be fitted to the following equation: $y = a_1 + b_1 \cdot \ln(x)$, where y corresponds to the intensity of the TL signal, x is the time of irradiation, a_1 and b_1 are coefficients of the equation. It means that, from 40 min onwards there is a saturation process where the electron-hole recombinations reach the maximum efficiency regardless of the absorbed dose. As shown in Table 1, there is a significant difference for the GR-200 exposed from 10 to 50 min (Fig. 5d), where the evolution of the signal can be expressed as: $y = a_2 \cdot e^{\frac{x}{t}}$, where y corresponds to the intensity of the TL emission, x is the time of UVC exposure, a_2 and t are coefficients of the equation. Such behaviour could be associated with the phototransfer process that dominates when the UVC exposure increases. In both cases, position of the peaks does not shift when the dose is increased, so the assumption of first order kinetics behaviour for the TL process is confirmed.

3.2.3. TL kinetic analysis

Both β and UVC radiations performed on TLD-100, TLD-200, TLD-400 and GR-200 display several differences in the UV-blue TL emission that are directly linked to the nature of the source. Samples show an acceptable radiation sensitivity with well-defined peaks, although each dosimeter displays glow curves that differs considerably in shape and intensity, caused by the different structure and the sort of dopants and can be studied by CGCD method. The glow curve is made up of individual glow peaks, which are, in principle, related to distinct trapping centers. Therefore, an understanding of the physical mechanisms underlying glow curves can only be obtained by decomposing the glow curve into its component glow peaks. Glow peaks are themselves complex issues, and are often simulated using a rather simplistic approach based on first order kinetics.

Deconvolution performed on the β irradiated TLDs matches with the parameters previously reported [31–33]. The identification of each peak is exhibited in Fig. 6 where it is possible to distinguish 5 maxima for both TLD-100 and TLD-200, 2 groups of components for TLD-400 and one peak for GR-200. Despite of TLD-100 and GR-200 have the same lattice (LiF) the presence of the dopants infer significant changes in the structure giving rise to significant differences in shape and intensity (three times higher for GR-200) of the TL glow curves. Similarly to TLD-200 and TLD-400 where the same matrix (CaF_2) containing different dopants (Dy and Mn, respectively) induce TL glow curves that differ in shape and intensity (two times higher for TLD-200).

As seen in Fig. 7, UVC exposure induces the activation of trap charges that are not involved when using ionizing radiation. All the materials modify drastically the shape of the TL curve probably associated with the combination of the partially ionizing effect, phototransfer process and bleaching effect of the UVC.

The TL kinetic parameters are shown in Tables 2 and 3 and it is possible to distinguish the activation of three traps at temperatures higher than 220 °C for TLD-100 with E_a values of 1.12, 1.54 and 1.69 eV and the bleaching of the peak 4 observed in the UVC-irradiated samples. The UVC effect on TLD-400 and GR-200 leads to the activation of low-temperature traps (T < 220 °C) without a well-defined TL structure that is analysed in terms of FOK giving rise to a complex structure consisting respectively of two and six components. However, the TL mechanism observed for TLD-200 seems to involve the same traps regardless of the type of the irradiation source in the range of 200–300 °C. The temperature at which the maximum intensity T_{max} (^oC) appears of every peak is related to the activation energy E (eV), the frequency factor s (s^{-1}) and the heating rate β ($s^{-1}.^oC$) (see **Eq. (6)**). Also, geometrically, the E parameter is strongly related to the width of every peak (keeping the asymmetry typical of the FOK approach). It means that it is possible to observe wider maxima peaked at higher temperature with E values lower than peaks appearing at lower temperature (i.e. TLD-200 after β radiation (Table 2) with Peak 4 at T_{max} = 205 °C and E_a = 0.78).

One can therefore conclude that TLD-200 appears as a suitable material to be employed for a ionizing and UVC dosimeter, but further work is necessary to confirm such an assertion. Nevertheless, and supported by Tables 2 and 3, one can compare the β and UVC radiation effect on the induced TL emission for each material.

Thus, TLD-100 **(**Fig. 6**a)** displays the typical UV-blue TL glow curve corresponding to 10 mGy β irradiated, which gives rise to five individual peaks centered at ~80 °C (peak 1), ~120 °C (peak 2), ~150 °C (peak 3), ~175 °C (peak 4) and ~200 °C (peak 5) that attending to the shape of the peaks one can consider as a good approach to first order kinetics process [30]. The appearance of these maxima should be due to (i) Ti^{4+}–OH^- defect complexes associated with Mg^{2+} vacancies (Mg-dipoles) for peak 1; (ii) Mg^{2+} dipoles corresponding to both peaks 2 and 3 and (iii) Ti^{4+}–OH^-/ Mg^{2+}-trimer defect complexes for peaks 4 and 5 (ratio of 2:5) [34]. Several studies [35] have shown that TLD-100 contains a high concentration of OH^- (1.37 Å of ionic radius) [36] substituting F^- (1.33 Å) [36] with similar masses and hence easily diffuse throughout the LiF lattice during crystal growth or by thermal annealing treatments. Such studies have also suggested that TL glow curve shapes and sensitivity for LiF:Mg,Ti, as well as complex natural and synthetic materials [37], are directly dependent on the OH^- concentration, since the metals in general and both Ti^{4+} and Mg^{2+} in particular for the TLD-100 are favourable to react with such hydroxyl groups. Consequently, the TL sensitivity of this material increases with the concentration of OH^- up to saturation of all Ti^{4+} [38]. The role of the hydroxyl groups in the luminescence emission has been previously observed for several

Table 1
Graphic fitting values of the dose response. β radiation fits linear equation: $y = a_0 + b_0 \cdot x$. UVC radiation on TLD-100, TLD-200 and TLD-400 fits saturation equation: $y = a_1 + b_1 \cdot ln(x)$. UVC radiation on GR-200 fits exponential equation: $y = a_2 \cdot e^{x/t}$ and r^2 corresponds to the regression coefficient.

	β radiation			**UVC radiation**					
	a_0	b_0	r^2	a_1	b_1	r^2	a_2	t	r^2
TLD-100	0.019	0.098	0.999	− 0.364	0.567	0.994	–	–	–
TLD-200	− 0.019	0.092	1	− 0.353	0.456	0.989	–	–	–
TLD-400	0.087	0.091	1	− 0.064	0.351	0.989	–	–	–
GR-200	1.981	0.285	0.996	–	–	–	0.141	28.329	0.999

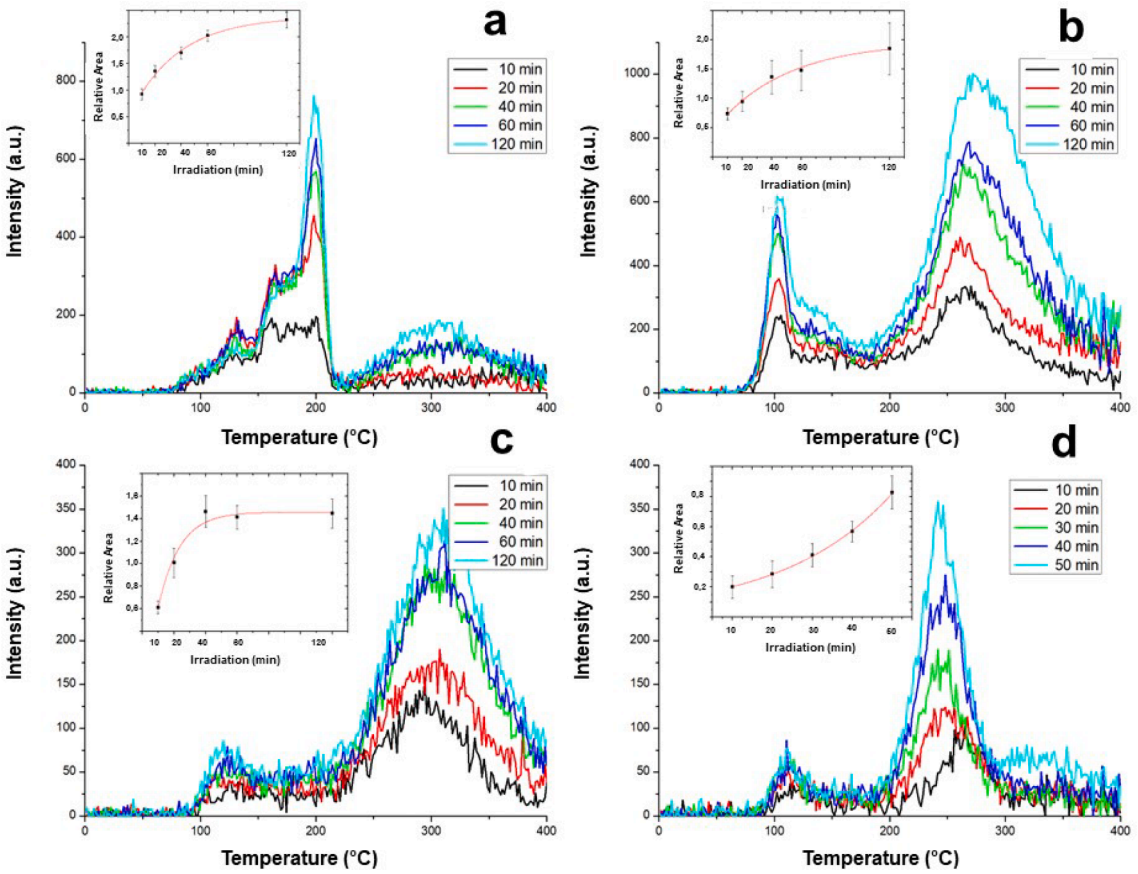

Fig. 5. Dose response of (a) TLD-100, (b) TLD-200 and (c) TLD-400 dosimeters exposed from 10 to 120 min of UVC radiation. And (d) GR-200 chip exposed from 10 to 50 min.

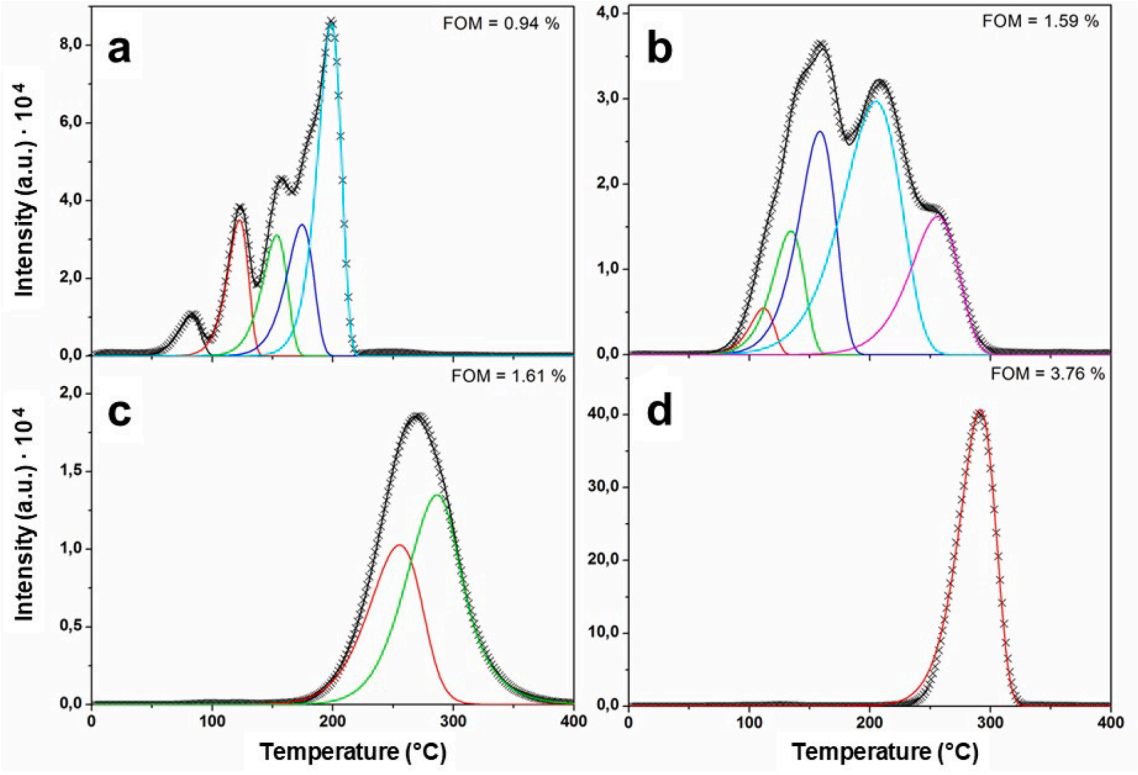

Fig. 6. Deconvolution of glow curves of (a) TLD-100, (b) TLD-200, (c) TLD-400 and (d) GR-200 dosimeters exposed to 10 mGy of β radiation.

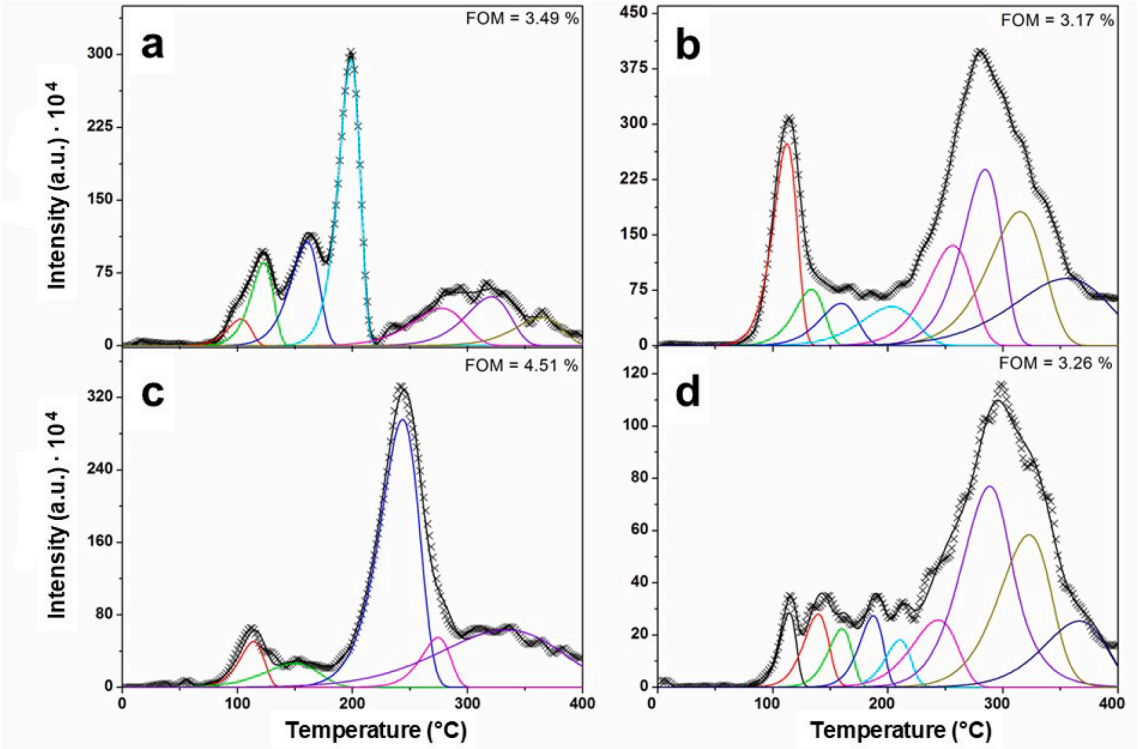

Fig. 7. Deconvolution of glow curves of (a) TLD-100, (b) TLD-200, (c) TLD-400 and (d) GR-200 dosimeters exposed to 40 min of UVC radiation.

Table 2
Kinetic parameters of the dosimeters after β radiation.

β radiation					
		E (eV)	I_{MAX} (a. u.)	T_{MAX} (°C)	S (s^{-1})
TLD-100	Peak 1	1.19 ± 0.06	10267 ± 72	82 ± 4	$3.92 \cdot 10^{16}$
	Peak 2	1.58 ± 0.08	35140 ± 165	123 ± 4	$4.20 \cdot 10^{19}$
	Peak 3	1.54 ± 0.08	31172 ± 157	154 ± 4	$4.33 \cdot 10^{17}$
	Peak 4	1.55 ± 0.08	33913 ± 586	175 ± 4	$6.46 \cdot 10^{16}$
	Peak 5	1.97 ± 0.01	85887 ± 800	199 ± 5	$2.86 \cdot 10^{20}$
TLD-200	Peak 1	1.24 ± 0.06	5485 ± 159	112 ± 4	$4.93 \cdot 10^{15}$
	Peak 2	1.09 ± 0.05	14534 ± 417	135 ± 4	$1.05 \cdot 10^{13}$
	Peak 3	1.03 ± 0.05	26219 ± 309	159 ± 4	$2.29 \cdot 10^{11}$
	Peak 4	0.78 ± 0.003	29689 ± 1423	205 ± 6	$3.94 \cdot 10^{8}$
	Peak 5	1.20 ± 0.07	19237 ± 1287	254 ± 6	$6.27 \cdot 10^{10}$
TLD-400	Peak 1	1.15 ± 0.06	9870 ± 738	259 ± 7	$2.94 \cdot 10^{10}$
	Peak 2	1.40 ± 0.07	11310 ± 846	283 ± 7	$2.32 \cdot 10^{12}$
GR-200	Peak 1	1.91 ± 0.01	407261 ± 20315	291 ± 6	$2.79 \cdot 10^{15}$

Table 3
Kinetic parameters of the dosimeters after UVC radiation.

UVC radiation					
		E (eV)	I_{MAX} (a. u.)	T_{MAX} (°C)	S (s^{-1})
TLD-100	Peak 1	1.18 ± 0.02	28 ± 8	103 ± 6	$3.48 \cdot 10^{15}$
	Peak 2	1.39 ± 0.02	86 ± 25	123 ± 2	$2.16 \cdot 10^{17}$
	Peak 3	1.30 ± 0.01	108 ± 33	160 ± 1	$5.54 \cdot 10^{14}$
	Peak 4	–	–	–	–
	Peak 5	2.08 ± 0.04	471 ± 143	199 ± 2	$8.90 \cdot 10^{21}$
	Peak 6	1.12 ± 0.01	39 ± 15	278 ± 9	$3.91 \cdot 10^{9}$
	Peak 7	1.54 ± 0.04	73 ± 24	321 ± 7	$3.08 \cdot 10^{12}$
	Peak 8	1.69 ± 0.04	29 ± 11	364 ± 8	$5.19 \cdot 10^{12}$
TLD-200	Peak 1	1.23 ± 0.06	274 ± 77	112 ± 5	$4.79 \cdot 10^{10}$
	Peak 2	1.10 ± 0.02	76 ± 37	134 ± 6	$1.42 \cdot 10^{13}$
	Peak 3	0.97 ± 0.02	57 ± 20	159 ± 6	$6.55 \cdot 10^{10}$
	Peak 4	0.79 ± 0.02	53 ± 20	203 ± 8	$5.89 \cdot 10^{7}$
	Peak 5	1.22 ± 0.01	135 ± 45	256 ± 4	$7.91 \cdot 10^{10}$
	Peak 6	1.53 ± 0.01	239 ± 88	284 ± 3	$1.23 \cdot 10^{13}$
	Peak 7	1.21 ± 0.01	181 ± 67	315 ± 3	$3.97 \cdot 10^{9}$
	Peak 8	0.77 ± 0.02	91 ± 34	355 ± 5	$2.33 \cdot 10^{5}$
TLD-400	Peak 1	1.21 ± 0.06	51 ± 10	114 ± 1	$1.18 \cdot 10^{14}$
	Peak 2	0.62 ± 0.03	26 ± 5	150 ± 1	$2.86 \cdot 10^{6}$
	Peak 3	1.34 ± 0.07	296 ± 58	244 ± 2	$4.23 \cdot 10^{12}$
	Peak 4	2.0 ± 0.1	55 ± 11	274 ± 3	$9.58 \cdot 10^{18}$
	Peak 5	0.55 ± 0.03	63 ± 12	334 ± 3	$3.53 \cdot 10^{3}$
GR-200	Peak 1	1.9 ± 0.1	28 ± 10	112 ± 4	$2.12 \cdot 10^{25}$
	Peak 2	1.47 ± 0.07	27 ± 11	136 ± 4	$5.70 \cdot 10^{17}$
	Peak 3	1.65 ± 0.08	22 ± 9	158 ± 4	$1.01 \cdot 10^{19}$
	Peak 4	1.87 ± 0.09	27 ± 10	187 ± 5	$1.44 \cdot 10^{20}$
	Peak 5	2.0 ± 0.1	17 ± 8	207 ± 5	$3.78 \cdot 10^{20}$
	Peak 6	1.19 ± 0.01	26 ± 11	241 ± 5	$1.27 \cdot 10^{11}$
	Peak 7	1.46 ± 0.07	65 ± 15	275 ± 5	$7.87 \cdot 10^{12}$
	Peak 8	1.43 ± 0.07	56 ± 11	315 ± 6	$3.98 \cdot 10^{11}$
	Peak 9	1.32 ± 0.07	25 ± 10	363 ± 6	$5.38 \cdot 10^{9}$

natural materials consisting of a faster return of the electrons to their ground inducing the emission of photons in the UV-blue region [39].

As shown in Fig. 7a, UV-induced glow emission of this material displays four peaks at ~100 °C (peak 1), ~120 °C (peak 2), ~160 °C (peak 3), ~200 °C (peak 5) similar to the ioizing irradiated sample and three maxima at ~280 °C (peak 6), ~320 °C (peak 7) and ~365 °C (peak 8) that seems to be mainly linked to the non-ionizing component of the UVC exposure. All of them exhibit first order kinetics behaviour indicating that the TL process involves the same traps regardless of the type of the source in the range of RT-250 °C (i.e. the defects concerning such emission are identical). Respect to the lowest temperature TL UV-blue peak 1 at ~70 °C in Fig. 6a, is usually not detected due to the high probability of the peak electron release from the shallower traps at RT

and the higher temperature broad maximum in Fig. 7a (consisting of three peaks) is clearly caused by the non-ionizing component of the 254.7 nm exposure [40]. Therefore, TLD-100 should be a suitable not only as ionising radiation dosimeter, but also as UVC detector due to the appeareance of the high temperature signal over ~290 °C.

As appreciated in Fig. 6b, the 10 mGy-β irradiated TLD-200 glow curve consists of a group of five overlapped components at ~110 °C (peak 1), ~135 °C (peak 2), ~160 °C (peak 3), ~205 °C (peak 4) and ~255 °C (peak 5). These maxima are associated with structural defects and impurities due to the aforementioned Dy^{3+} ions (with atomic radii of 1.59 Å). Several studies declared five [41], six [42] using beta irradiation and the T_m-T_{stop} method to determine the trap system of the components involved in the luminescent process. Furthermore, Yazici et al. [29], claimed that the kinetic order of the TLD-200 is not constant and is directly dependent on the annealing time due to the continuum distribution of belonging traps.

However, the UV-induced TL glow emission of the TLD-200 (Fig. 7b) has been scarcely studied and exhibits eight peaks at ~110, ~135, ~160, ~200, ~255, ~285, ~315 and ~355 °C. One can observe how the lower temperature TL emission, at ~110 °C (similarly to the beta induced TL signal, Fig. 6b), is masked due to the differences of the relative intensities caused by both radiation sources. This maximum appears with less relative intensity value respect to the peak after β irradiation (ratio of 1:18), which exhibits the higher sensitivity to ionizing radiation. Peaks 2, 3 and 4 are linked to the bleaching effect of the UVC light on the TL signal. On the contrary, peaks 5 to 8 are directly asociated with the ionizing component of the UVC and/or with the beta source. Therefore, TLD-200 could allow us to discriminate between UVC or ionizing radiation taking into account the presence of the TL signal in the range of 120–220 °C.

The β-irradiated TLD-400 (Fig. 6c) is characterized by a broad maximum centered at ~290 °C that can be deconvoluted into two components peaked at ~260 and ~280 °C that would be related to structural defects and Mn^{2+} impurities (with atomic radii of 1.17 Å) that are placed in Ca^{2+} sites (1.74 Å) in the crystal lattice [9]. Although TLD-400 shows high sensitivity to the ionizing radiation at temperatures above 200 °C, the TL signal is almost negligible at lower temperatures. According to Topaksu et al., [9], this complex TL glow curve could not be analyzed assuming the model based on the discrete trap distribution, so such an assertion could be explained by the T_m-T_{stop} method which indicates the presence of close overlapping groups of components probably associated with a continuum in the trap distribution rather than a discrete trapping level. On the other hand, Fig. 7c displays the UV-induced glow curve of TLD-400 giving rise to several emissions up to 200 °C which are linked to UVC radiation and a broad maximum centered at ~300 °C that can be deconvolutes into three components centered at ~240, 275 and 335 °C associated with the ionizing radiation (beta source). Consequently, TLD-400 would be a suitable dosimeter to detect UVC radiation due to the presence of TL signal up to 200 °C.

The TL glow curve of 10 mGy beta irradiated GR-200 (Fig. 6d) displays only one maximum centered at ~290 °C (peak 1), which is considered in terms of the recombination of both H-F defects and V_k-e centers [43]. Thus, GR-200 shows much more sensitivity to radiation ~32000 a.u.) in contrast to the other dosimeters used in the present work measured under the same conditions (i.e. TLD-100, TLD-200 and TLD-400). As appreciated in Fig. 7d, such sensitivity to the ionizing radiation appears at higher temperatures (up to 200 °C) with a negligible response at lower temperatures. According to Horowitz et al., [44], this dosimetric peak is linked to a first-order kinetics based on computerised glow curve analyse (CGCA). So, GR-200 could be a suitable dosimeter to detect ionizing radiation, whereas that it could not discriminate between UVC and ionizing radiation. The complex glow curve analysis observed in Fig. 7d, consisting of nine groups of components, supports this assertion.

4. Conclusions

Based on their luminescence properties, we can conclude that TLD-100, TLD-200, TLD-400 and GR-200 dosimeters could be potentially used in the field of UV Dosimetry. CL emissions of these synthetic dosimeters differ considerably in shape and intensity due to their chemical compositions: TLD-100 and GR-200 display three groups of components consisting on: (i) a broad band in the range of 300–450 nm (intrinsic emission of LiF); (ii) a green waveband (F_3^+ emission band) and (iii) the red-infrared emission band (F_2 centres). On the other hand, TLD-200 displays well-defined peaks that could specifically be associated with the CaF_2 lattice and point depects (from 450 to 800 nm) linked to the Dy^{3+} transitions, where the magnetic dipole transition ($^4F_{9/2} \rightarrow {}^6H_{15/2}$) predominates against the electric dipole transition. And TLD-400 only displays a waveband centered at 490 nm that could be linked to Mn^{2+} impurities ($^4T_{1g} \rightarrow {}^6A_{1g}$ transition) in the CaF_2 lattice. The TL kinetic analysis obtained by deconvolution of glow curves shows that UVC exposure induces the activation of trap charges that are not involved when using ionizing radiation; i.e. there is a change in shape of the glow curves and in the groups of components involved in the luminescence mechanism. This can be explained with the combination of the partially ionizing effect, phototransfer process and bleaching effect of the UVC radiation. Based on their spectral UVC induce TL responses, (i) TLD-100 and TLD-400 could be suitable UVC detectors due to their TL signals at high temperatures ~292 °C and up to 200 °C, respectively); (ii) TLD-200 could allow us to discriminate between UVC or ionizing radiation taking into account the presence of the TL emission in the range of 120–220 °C. However, GR-200 could not allow us to discriminate between UVC and ionizing radiation.

Moreover, β-irradiated dose response fits to a linear equation without sub or supralinearity in the range of 10–80 mGy, however UVC radiation saturates in TLD-100, TLD-200 and TLD-400 from 40 min onwards up to 120 min of exposure, although a linear behaviour can be observed at lower exposure times (up to 40 min). On the other hand, GR-200 shows an exponential evolution due to phototransfer process dominating when the dose increases. The stability of the TL signal displays significant scattering when the samples are UVC irradiated in both cycles and aliquots. TLD-200 potentially appears as the most acceptable dosimeter under these conditions since there is not an eviction nor an increase of electrons or holes from the ground state to non-radiative recombination centers. Nevertheless, further work is necessary to confirm such an assertion.

CRediT authorship contribution statement

C. Boronat: Investigation. **V. Correcher:** Investigation, Supervision. **J.C. Bravo-Yagüe:** Investigation, Supervision. **I. Sarasola-Martin:** Investigation. **J. Garcia-Guinea:** Investigation. **J.F. Benavente:** Investigation.

Declaration of Competing Interest

The authors declare that they have no known competing financial interests or personal relationships that could have appeared to influence the work reported in this paper.

Data availability

Data will be made available on request.

References

[1] R. Nagaraj, V. Rajagopal, A. Raja, S. Ranjith, Influence of Dy^{3+} ion concentration on photoluminescence and energy transfer mechanism of promising $KBaScSi_3O_9$ phosphors for warm white LEDs, Spectrochim, Acta, Part A. 264 (2022), 120212, https://doi.org/10.1016/j.saa.2021.120212.

[2] C. Zhou, Y. Zhang, J. Zhu, X. Ren, Y. Zhu, P. Yin, L. Zhao, J. Wang, X. Feng, Enhanced luminescence performances of $BaLaMgTaO_6$: Mn^{4+} red phosphor by Bi^{3+}, Ca^{2+} doping for indoor plant lighting supplementary LED, Spectrochim, Acta, Part A. 268 (2022), 120655, https://doi.org/10.1016/j.saa.2021.120655.

[3] Y. Chen, X. Yu, Y. Jiang, M. Liu, Z. Chen, L. Ding, B. Li, C. Zeng, Highly sensitive sensing device based on highly luminescent lanthanide nanocluster for biomarker in human urine and serum, Spectrochim, Acta, Part A. 270 (2022), 120782, https://doi.org/10.1016/j.saa.2021.120782.

[4] J. Zhang, X. Zhou, J. Wang, D. Fang, A red-emitting Europium(III) complex as a luminescent probe with large Stokes shift for the sequential determination of Cu^{2+} and biothiols in real samples, Spectrochim, Acta, Part A. 282 (2022), 121663, https://doi.org/10.1016/j.saa.2022.121663.

[5] X. Piao, T. Guo, Z. Zou, J. Liao, H. Wen, G. Guoliang, Site-splitting inhibition and near-infrared luminescence properties of Cr^{3+} activated magnetoplumbite $SrAl_{12}O_{19}$ modified by La and Mg, Spectrochim, Acta, Part A. 281 (2022), 121602, https://doi.org/10.1016/j.saa.2022.121602.

[6] Y. Meng, N. Zhang, J. Li, Y. Xu, Q. Yang, Y. Yuan, X. Zhang, J. Wu, L. Zhao, The detection of selectivity and sensitivity towards TNP by a new Zn(II)-coordination polymer as luminescent sensor in aqueous solution, Spectrochim, Acta, Part A. 266 (2022), 120419, https://doi.org/10.1016/j.saa.2021.120419.

[7] S.W.S. McKeever, Mechanisms of thermoluminescence production in materials for radiation dosimetry, Radiat. Prot. Dosim. 17 (1986) 431–435, https://doi.org/10.1093/oxfordjournals.rpd.a079854.

[8] P.S. Weng, S.H. Li, P.C. Hsu, K.C. Hsu, Response of thermoluminescent dosimeter CaF_2: Dy to ionizing and non-ionizing radiations, Int. J. Radiat. Phys. Chem. 43 (1992) 717–720, https://doi.org/10.1016/0883-2889(92)90232-4.

[9] M. Topaksu, V. Correcher, J. Garcia-Guinea, Luminescence emission of natural fluorite and synthetic CaF_2: Mn (TLD-400), Radiat. Phys. Chem. 119 (2016) 151–156, https://doi.org/10.1016/j.radphyschem.2015.10.002.

[10] D. Wróbel, P. Bilski, B. Marczewska, A. Mrozik, M. Kłosowski, Characterization of the Risø TL/OSL DA-20 reader for application in TL dosimetry, Radiat. Meas. 74 (2015) 1–5, https://doi.org/10.1016/j.radmeas.2014.12.011.

[11] M. Pagel, V. Barbin, P. Blanc, D. Ohnenstetter, Cathodoluminescence in Geosciences, fisrt ed., Springer-Verlag, Berlin Heidelberg GmbH, 2000.

[12] E. Bulur, Photo-transferred luminescence from BeO ceramics, Radiat. Meas. 42 (2007) 334–340, https://doi.org/10.1016/j.radmeas.2007.02.065.

[13] V. Correcher, C. Boronat, M.D. Virgos, J. Garcia-Guinea, UV-Induced Thermoluminescence of Natural Ca-Rich Carbonates, J. Appl. Spectrosc. 86 (2020) 1004–1009, https://doi.org/10.1007/s10812-020-00931-5.

[14] M. Topaksu, V. Correcher, C. Boronat, J. Garcia-Guinea, Z.G. Portakal, S. Akça, UV effect on the cathodo- and thermoluminescence properties of a gem-quality Cr-rich diaspore (α-AlOOH), Appl. Radiat. Isot. 141 (2018) 101–106, https://doi.org/10.1016/j.apradiso.2018.08.025.

[15] L. Bøtter-Jensen, G.A.T. Duller, A new system for measuring optically stimulated luminescence from quartz samples, Nucl. Tracks Radiat. Meas. 20 (1992) 549–553, https://doi.org/10.1016/1359-0189(92)90003-E.

[16] A. Delgado, V. Unamuno, J.L. Muñiz, V. Correcher, J.M. Gómez Ros, A simple UV irradiator for low dose reassessment with LiF TLD-100, Radiat. Prot. Dosim. 67 (1996) 303–306, https://doi.org/10.1093/oxfordjournals.rpd.a031834.

[17] J.F. Benavente, J.M. Gómez-Ros, A.M. Romero, Thermoluminescence glow curve deconvolution for discrete and continuous trap distributions, Appl. Radiat. Isot. 153 (2019), 108843, https://doi.org/10.1016/j.apradiso.2019.108843.

[18] I. Tale, M. Springis, U. Rogulis, V. Ogorodnik, P. Kulis, V. Tale, A. Veispals, H. J. Fitting, Self-trapped holes and recombination luminescence in $LiBaF_3$ crystals, Radiat. Meas. 33 (2001) 751–754, https://doi.org/10.1016/S1350-4487(01)00096-8.

[19] B. Yang, B.J. Luff, P.D. Townsend, Cathodoluminescence spectra of pure LiF, Nucl. Instrum. Methods Phys. Res., Sect. B. 65 (1992) 497–501, https://doi.org/10.1016/0168-583X(92)95093-7.

[20] T. Kuliński, F. Kaczmarek, M. Ludwiczak, Z. Błaszczak, Emission characteristics of an LiF: F_2 colour centre laser in the visible, Opt. Commun. 35 (1980) 120–124, https://doi.org/10.1016/0030-4018(80)90373-9.

[21] L. Qi, M. Guo, L. Han, H. Gu, Electrolytic coloration and spectral properties of O^{2-} and Mg^{2+}-codoped LiF crystals, Spectrochim. Acta, Part A 152 (2016) 438–442, https://doi.org/10.1016/j.saa.2015.07.059.

[22] M. Izerrouken, A. Meftah, M. Nekkab, Color centers in neutron-irradiated $Y_3Al_5O_{12}$, CaF_2 and LiF single crystals, J. Lumin. 127 (2007) 696–702, https://doi.org/10.1016/J.JLUMIN.2007.04.005.

[23] C. Boronat, T. Rivera, J. Garcia-Guinea, V. Correcher, Cathodoluminescence emission of REE (Dy, Pr and Eu) doped $LaAlO_3$ phosphors, Radiat. Phys. Chem. 130 (2017) 236–242, https://doi.org/10.1016/j.radphyschem.2016.09.005.

[24] A.H. Qaisi, U.H. Kaynar, M. Ayvacikli, J. Garcia-Guinea, Y. Alajlani, M. Topaksu, N. Can, Novel Dy incorporated $Ca_3Y_2B_4O_{12}$ phosphor: Insights into the structure, broadband emission, photoluminescence and cathodoluminescence characteristics, Appl. Radiat. Isot. 185 (2022), 110257, https://doi.org/10.1016/J.APRADISO.2022.110257.

[25] Ü.H. Kaynar, S. Cam Kaynar, Y. Alajlani, M. Ayvacikli, E. Karali, Y. Karabulut, S. Akca, T. Karali, N. Can, Eu^{3+} and Dy^{3+} doped La_2MoO_6 and $La_2Mo_2O_9$ phosphors: Synthesis and luminescence properties, Mater. Res. Bull. 123 (2020), 110723, https://doi.org/10.1016/J.MATERRESBULL.2019.110723.

[26] W.Y. Shen, M.L. Pang, J. Lin, J. Fang, Host-Sensitized Luminescence of Dy^{3+} in Nanocrystalline β-Ga_2O_3 Prepared by a Pechini-Type Sol-Gel Process, J. Electrochem. Soc. 152 (2005) 25–28, https://doi.org/10.1149/1.1847674.

[27] P.D. Sahare, M. Singh, P. Kumar, Synthesis and TL characteristics of MgB_4O_7:Mn, Tb phosphor, J. Lumin. 160 (2015) 158–164, https://doi.org/10.1016/j.jlumin.2014.11.042.

[28] L. Oster, Y.S. Horowitz, A. Horowitz, Glow curve readout of LiF:Mg, Cu, P (GR-200) chips at maximum temperatures between 240°C and 280°C: Elimination of the residual signal, Radiat. Prot. Dosim. 49 (1993) 407–411, https://doi.org/10.1093/oxfordjournals.rpd.a081980.

[29] E.A. Ainsbury, D. Samaga, S. della Monaca, M. Marrale, C. Bassinet, C.I. Burbidge, V. Correcher, M. Discher, J. Eakins, P. Fattibene, I. Güçlü, M. Higueras, E. Lund, N. Maltar-Strmečki, S. McKeever, C.L. Rääf, S. Sholom, I. Veronese, A. Wieser, C. Woda, F. Trompier, Uncertainty on radiation doses estimated by biological and retrospective physical methods, Radiat. Prot. Dosim. 178 (2018) 382-404. Doi:10.1093/rpd/ncx125.

[30] C.M. Sunta, S.P. Kathuria, Order of kinetics for thermoluminescence in LiF (TLD-100), J. Phys. D: Appl. Phys. 16 (1983) 163–164, https://doi.org/10.1088/0022-3727/16/8/005.

[31] A.N. Yazici, M. Bedir, A.S. Sökücü, The analysis of dosimetric thermoluminescent glow peak of CaF_2:Mn after β-irradiation, Nucl. Instrum. Methods Phys. Res., Sect. B. 259 (2007) 955-965. Doi:10.1016/j.nimb.2007.02.104.

[32] A. Necmeddin Yazici, R. Chen, S. Solak, Z. Yegingil, The analysis of thermoluminescent glow peaks of CaF_2: Dy (TLD-200) after β-irradiation, J. Phys. D: Appl. Phys. 35 (2002) 2526–2535, https://doi.org/10.1088/0022-3727/35/20/311.

[33] P. Bilski, Lithium fluoride: From LiF:Mg, Ti TO LiF:Mg, Cu, P, Radiat. Prot. Dosim. 100 (2002) 199–206, https://doi.org/10.1093/oxfordjournals.rpd.a005847.

[34] J.S. Dryden, B. Shuter, The dependence of the thermoluminescence of LiF: Mg^{2+} crystals on the state of aggregation of the Mg^{2+} ions, J. Phys. D: Appl. Phys. 6 (1973) 123–130, https://doi.org/10.1088/0022-3727/6/1/316.

[35] D. Weiss, Y.S. Horowitz, L. Oster, Delocalized recombination kinetic modeling of the LiF:Mg, Ti (TLD-100) glow peak 5 TL system, Radiat. Meas. 43 (2008) 254–258, https://doi.org/10.1016/j.radmeas.2007.10.026.

[36] R.D. Shannon, Revised effective ionic radii and systematic studies of interatomic distances in halides and chalcogenides, Acta Crystallogr, Sect. A: Found. Crystallogr. 32 (1976) 751–767, https://doi.org/10.1107/S0567739476001551.

[37] V. Correcher, J.M. Gómez-Ros, J. Garcia-Guinea, A. Delgado, Thermoluminescence kinetic parameters of basaltic rock samples due to continuous trap distribution, Nucl. Instrum. Methods Phys. Res., Sect. A. 528 (2004) 717–720, https://doi.org/10.1016/j.nima.2004.04.208.

[38] W. Wachter, N.J. Vana, H. Aiginger, The influence of hydroxyl ions on the thermoluminescence properties of LiF: Mg, Ti, Nucl. Instrum. Methods. 175 (1980) 21–23, https://doi.org/10.1016/0029-554X(80)90239-6.

[39] J. Garcia-Guinea, F. Garrido, P. Lopez-Arce, V. Correcher, J. de la Figuera, Spectral green cathodoluminescence emission from surfaces of insulators with metal-hydroxyl bonds, J. Lumin. 190 (2017) 128–135, https://doi.org/10.1016/j.jlumin.2017.05.039.

[40] B. Chandra, A.R. Lakshmanan, R.C. Bhatt, Effect of deep traps on sensitization in LiF (TLD-100) phosphor a correlation study between peak 7 and 10 centres, Phys. Status Solidi A. 66 (1981) 335–340, https://doi.org/10.1002/pssa.2210660141.

[41] G. Kitis, F. Hasan, M. Tsakiri, S. Charalambous, Implication of regenerated thermoluminescence on low dose measurements, Nucl. Tracks Radiat. Meas. 10 (1985) (1982) 571–574, https://doi.org/10.1016/0735-245X(85)90059-6.

[42] T.K. Wang, P.C. Hsu, P.S. Weng, Application of TLD-200 Dosemeters to the Discrimination of Alpha, Beta and Gamma, Radiat. Prot. Dosim. (1986) 225–230, https://doi.org/10.1093/oxfordjournals.rpd.a079750.

[43] B. Yang, L. Wang, P.D. Townsend, H. Gao, Comparison between the low temperature thermoluminescence spectra in annealed LiF:Mg,Cu, LiF:Mg,Cu,P and LiF:Mg,Cu,Si, Nucl. Instrum. Methods Phys. Res., Sect. B. 266 (2008) 2581-2586. Doi:10.1016/j.nimb.2008.03.199.

[44] Y.S. Horowitz, M. Moscovitch, Highlights and pitfalls of 20 years of application of computerised glow curve analysis to thermoluminescence research and dosimetry, Radiat. Prot. Dosim. 153 (2013) 1–22, https://doi.org/10.1093/rpd/ncs242.